

Effects of high-energy proton irradiation on separate absorption and multiplication GaN avalanche photodiode

Gui-Peng Liu¹ · Xin Wang¹ · Meng-Nan Li² · Zheng-Peng Pang¹ · Yong-Hui Tian¹ · Jian-Hong Yang¹

Received: 27 February 2018 / Revised: 29 April 2018 / Accepted: 2 May 2018 / Published online: 28 August 2018
© Shanghai Institute of Applied Physics, Chinese Academy of Sciences, Chinese Nuclear Society, Science Press China and Springer Nature Singapore Pte Ltd. 2018

Abstract The effect of high-energy proton irradiation on GaN-based ultraviolet avalanche photodiodes (APDs) is investigated. The dark current of the GaN APD is calculated as a function of the proton energy and proton fluences. By considering the diffusion, generation–recombination, local hopping conductivity, band-to-band tunneling, and trap-assisted tunneling currents, we found that the dark current increases as the proton fluence increases, but decreases with increasing proton energy.

Keywords Proton irradiation · GaN avalanche photodiode (APD) · Dark current · Detectors

1 Introduction

Gallium nitride (GaN) and its related compounds (AlGaN) are significant semiconductor materials in optoelectronic devices [1]. As wide band-gap semiconductors, GaN materials have been attracting a great deal of attention

in high-sensitivity ultraviolet (UV) detection [2]. GaN ultraviolet detection technology is widely used in the military and civil fields, such as ultraviolet communication, biochemical analysis, and other special applications [3, 4]. In some extremely harsh environment applications (e.g., satellites, radiation in the medical field, and nuclear power station) [2], it is always desirable to use materials with higher stabilities and radiation tolerances in optoelectronic devices to collect and process data. GaN is an excellent candidate material because of its strong anti-radiation ability [5]. Therefore, the effects of irradiation on GaN photoelectric detectors have received increasing attention.

It is well known that high-energy protons are the most important component of the space radiation environment. Therefore, the radiation damage to devices is mainly caused by energetic protons [6]. Significant efforts have been made to study the effects of proton irradiation on devices. In this paper, we study the effects of high-energy proton irradiation on a GaN ultraviolet avalanche photodiode (APD). Compared to the fragile and bulky photomultiplier tubes, GaN-based APDs have unique advantages, such as low dark current density, large internal gain, and solar-blind properties for ultraviolet detection [7]. In the past few years, GaN ultraviolet detectors have prompted great research interest. For example, Zhou et al. [8] demonstrated Schottky-type ultraviolet photodetectors based on an n-GaN substrate with an ultralow dark current of 0.56 pA at -10 V reverse bias. Pau et al. [9] demonstrated that the dark current of the back-illuminated GaN-based APD remains less than 1 pA for bias voltages less than 30 V, and the maximum multiplication gain is up to 41,200. More recently, Ji et al. [10] demonstrated a low leakage current density of a SAM APD of less than 1 nA/cm², with a large avalanche gain greater than 8.0×10^5 at

This work was supported by the National Natural Science Foundation of China (No. 61404132) and the Fundamental Research Funds for the Central Universities (Nos. lzujbky-2015-302, lzujbky-2017-171, and lzujbky-2016-119).

✉ Gui-Peng Liu
liugp@lzu.edu.cn

✉ Jian-Hong Yang
yangjh@lzu.edu.cn

¹ Institute of Microelectronics, School of Physical Science and Technology, Lanzhou University, Lanzhou 730000, China

² China Academy of Electronic and Information Technology, Beijing 100041, China

a reverse bias higher than 75 V. GaN APDs are always applied to flame and environmental monitoring and optical communication [11]. In this study, we analyzed the response of a GaN-based APD exposed to proton irradiation with different energies and proton fluences.

2 Model and methodology

The structure diagram of the separate absorption and multiplication (SAM) GaN APD is shown in Fig. 1. From bottom to top of the schematic cross section, the n-type contact, absorption, charge, multiplication, and p-type contact layers are shown. Different from traditional p-i-n structures, a thin n-type charge layer separates the absorption and multiplication layers, which can adjust the electric field distribution within the device. When the device is operated in the reverse bias, the direction of the electric field is directed from the n-type contact layer to the p-type contact layer, and the electric field in the multiplication layer is much larger than that in the absorption layer. Therefore, the SAM structure greatly improves the performance of the detector [12]. The parameters of the GaN APD used in this study are listed in Table 1.

The device irradiation damage mechanism can be simulated by Stopping and Range of Ions in Matter (SRIM). SRIM is the commonly used software for calculations of ion penetration in target materials [13]. Based on the binary collision approximation (BCA) method, SRIM uses a Monte Carlo algorithm, which can randomly sample the impact parameters of succeeding collisions based on the interaction cross section, composition, and atomic density of the target material. Until recently, corrections have been performed based on new experimental data [14], leading to

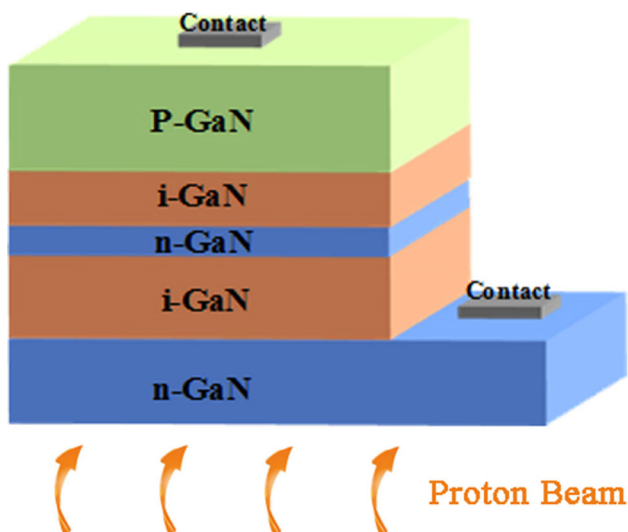


Fig. 1 Schematic of the photodetector used in this study

Table 1 Structural parameters of the GaN ultraviolet detector

Layer	Thickness (μm)	Doping (cm^{-3})
Au-contact	0.2	–
p-GaN	0.285	3×10^{18}
i-GaN	0.15	1×10^{16}
n-GaN	0.05	2×10^{18}
i-GaN	0.25	1×10^{16}
n-GaN	0.2	2×10^{18}

continued significant improvements in the SRIM simulation accuracy. Kim et al. [15] also demonstrated that the results regarding the energy loss and vacancy density as a function of target depth simulated by SRIM are in good agreement with the experiment results. In this letter, we use the SRIM software to simulate the process of an energetic proton beam flowing into the GaN ultraviolet detector, vertically from bottom to top. The interaction between incident particles and devices will produce Frenkel pairs in the Ga and N sublattices, causing deep trap levels in the material by the vacancies and interstitial atoms. The density and distribution of defects will affect the dark current of the GaN APD [16].

3 Simulation and calculation

The electrical and optical degradation in material properties is mainly due to atomic displacements and carrier trapping [16]. For GaN SAM APDs, the multiplication region and absorption region occupy the main part of the device. In addition, they are the most important operating areas for the device, which can seriously influence the properties of the device, especially in the high electric field region. Therefore, we focus on the Ga and N vacancies of the multiplication and absorption regions, respectively, irradiated by high-energy protons. We can use SRIM to extract the vacancy production rate in any position of the device at different incident energies. The vacancy density is the product of the production rate and proton fluences.

Figure 2 shows the density of the Ga and N vacancies caused by irradiation with 500 keV and 3 MeV of proton energies. In Fig. 2a, b, the density of the Ga vacancy is always greater than that of N vacancy, whether in the multiplication or absorption regions with different proton energies. The parameters extracted from the SRIM are shown in Table 2. The lattice binding energy is defined as the minimum energy required to remove an atom from the crystal lattice, which is equal between Ga and N atoms. The surface binding energy is always less than the lattice binding energy because the target atoms in the interface are

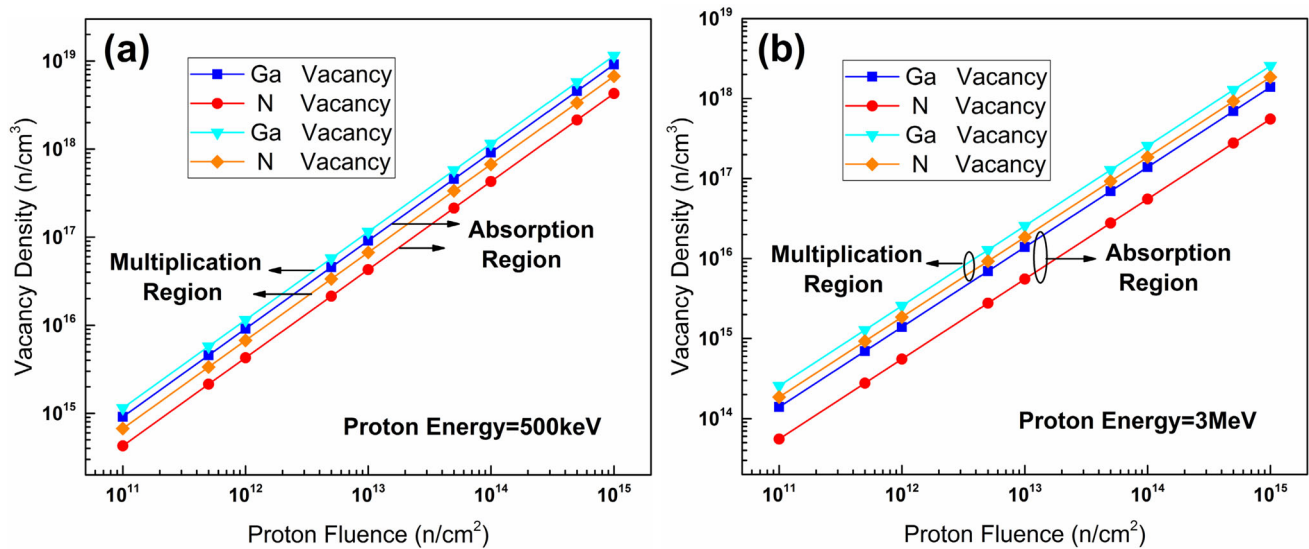


Fig. 2 Vacancy density in the multiplication and absorption regions for proton energies of **a** 500 keV and **b** 3 MeV

Table 2 Important energy values of the Ga and N atoms

	Ga	N
Lattice binding energy (eV)	3	3
Surface binding energy (eV)	2.82	2
Displacement energy (eV)	25	28

not bound near the surface, and the surface binding energy of the Ga atoms is slightly less than that of the N atoms. The displacement energy is the minimum energy required to strike a target atom from its crystal lattice position for a sufficient time that it cannot return quickly. In Table 2, the displacement energy of the Ga atoms is smaller than that of the N atoms, with a difference of 3 eV. For this reason, the Ga vacancy density is larger than that of N with different areas and different proton energies in the same position.

The high-energy protons enter the GaN APD devices, and the energy decreases due to the interaction between lattice atoms. The energy loss occurs in two forms: ionizing energy loss (IEL) and non-ionizing energy loss (NIEL). The IEL refers to the energy loss associated with ionization due to the inelastic collisions between protons and extranuclear electrons. The NIEL is a quantity that describes the energy loss of high-energy protons that produce target atomic displacements as they pass through the material. The NIEL calculations have been very useful for correlating radiation-induced device degradation. As a consequence, we paid more attention to the NIEL in this study.

Using the modified Kinchin–Pease relationship, we can obtain the relationship between the NIEL and vacancy formation rate [17]:

$$N_d = 0.8 \frac{E_n}{2T_d}, \tag{1}$$

where T_d is the threshold energy for atomic displacement, N_d is the number of atomic displacements in a unit distance, and E_n is the quantity of non-ionizing energy. The displacement energy for Ga and N atoms is listed in Table 2.

Figure 3a shows the total vacancy density versus the proton penetration depths at a fluence of 10^{13} n/cm² for different proton energies. Using the vacancy production rate and Eq. (1), the relationship between the NIEL and penetration depth is shown in Fig. 3b. With increasing proton energy, the radiation damage region becomes wider. The NIEL penetrates through the whole device when the proton energy is greater than 200 keV. In addition, at the same depth of the device, the higher proton energy corresponds to a smaller vacancy density and the NIEL. These trends are in good agreement with the results reported in the previous literature [15, 18]. The protons are quite heavy particles and travel in the material almost in a straight line. The higher the incident energy, the smaller the cross section between the incident proton and target nucleus, and the average energy transferred to the target nucleus decreases [16]. Because the device is very thin, the proton energy is sufficient to penetrate when the incident energy is 200 keV. When the proton energy is 500 keV, much greater than 200 keV, protons pass through the device at a higher speed and penetrate deeper. The interaction between protons and target atoms is very small and the corresponding NIEL decreases. Because the NIEL is already very small when the proton incident energy is 500 keV, the NIEL is reduced when the incident energy reaches 1000 keV, but does not vary considerably.

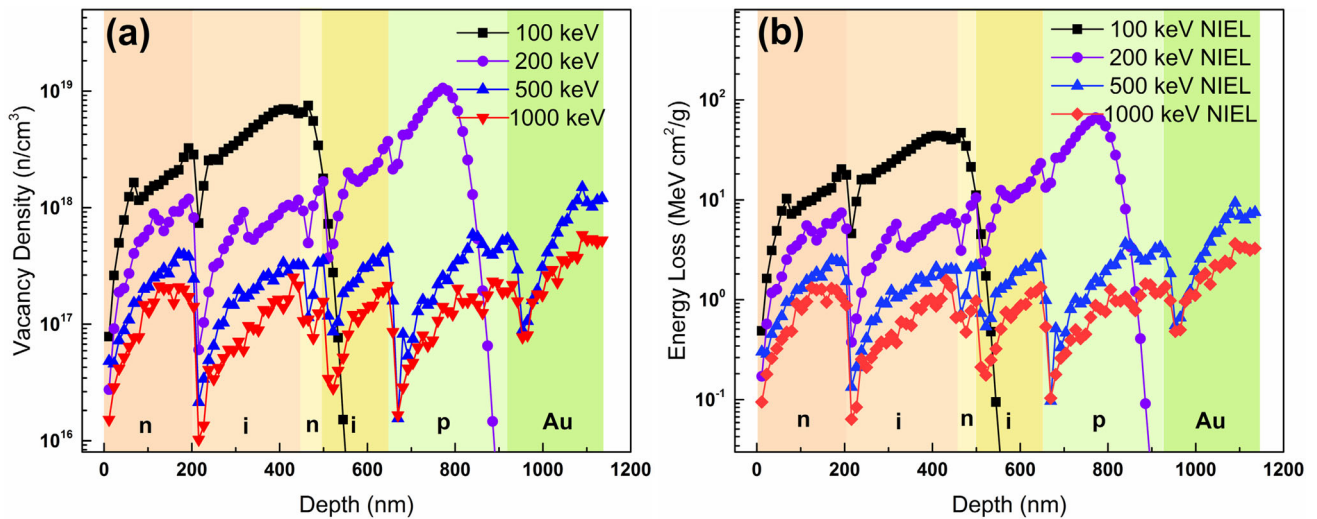


Fig. 3 **a** Vacancy density and **b** non-ionizing energy loss versus the penetration depth of the protons

Conversely, it was clearly observed that the NIEL is not continuous along the particle trajectories as the NIEL of the proton is reduced at the interface of each layer in the device. The detector contains five layers and a 200-nm thickness Au electrode, with six layers in total. Therefore, the NIEL divides into six segments with different thicknesses of each layer in the device. The NIEL in each layer increases with depth, before quickly declining in each interface. At the junction of each layer, the surface binding energy is less than the lattice binding energy inside of the material. As a result, the energy required to cause atomic displacements decreased, and it was expected that the NIEL would decrease dramatically in each interface. It is well known that the NIEL is always proportional to the proton-induced displacement damage in semiconductor devices [17, 19]. As a result, the total vacancy density is plotted versus depth in Fig. 3a, consistent with the NIEL versus depth plot in Fig. 3b.

4 Results and discussion

The *I*–*V* characteristic curve, in particular the dark current, is an important characterization of the detectors performance. In this study, we have assumed that the mechanisms of the dark current consisted of the diffusion current, the generation–recombination (G–R) in the depletion region, local hopping conductivity, band-to-band tunneling of carriers, and trap-assisted tunneling mechanism. As a result, the total dark current is the sum of the currents caused by the above mechanisms.

The diffusion current density, which is extremely small but always exists, is given by the expression [20]

$$J_{\text{diff}} = q \left(\frac{D_p}{L_p} p_n + \frac{D_n}{L_n} n_p \right) (1 - \exp(qV/2kT)), \tag{2}$$

where D_p (D_n) and L_p (L_n) are the diffusion coefficient and diffusion length of holes (electrons), respectively; p_n is the concentration of holes in the n-type region; n_p is the concentration of electrons in the p-type region; q is the charge of the electron; V is the applied voltage (assumed positive under reverse bias); and k is Boltzmann’s constant.

Similar to the diffusion current, the generation–recombination current is also small in wide-gap semiconductors and is given by the well-known relationship [21]

$$J_{\text{gen}} = \frac{qn_i W}{\tau_{\text{eff}}} (1 - \exp(qV/2kT)), \tag{3}$$

where n_i is the intrinsic carrier concentration, W is the width of the depletion region, and τ_{eff} is the minority carrier effective lifetime.

By considering the inevitable impurities and defects in the growth process, and traps induced by irradiation in the device, we introduce the local hopping conductivity model to ensure that the calculation results are more consistent with the experiment results. The model of dispersive transport in semiconductors with a high density of localized states in the band gap has been proposed [22, 23]. In this model, the electrons are captured to deep states and continue hopped motion via localized states before their recombination with holes. The carriers hopping motion becomes an important part of the recombination current. The hopping conductivity current density is [24]

$$J_{\text{hop}} = q^2 g(E_t) R_{ij}^2 v_{\text{hop}} E. \tag{4}$$

Here, $g(E_t) = (N_t/E_U) \exp(-E_t/E_U)$ is the distribution of energy of localized states near the conduction band; $E_U = 0.05$ eV is the Urbach energy [25]; R_{ij} is the distance the

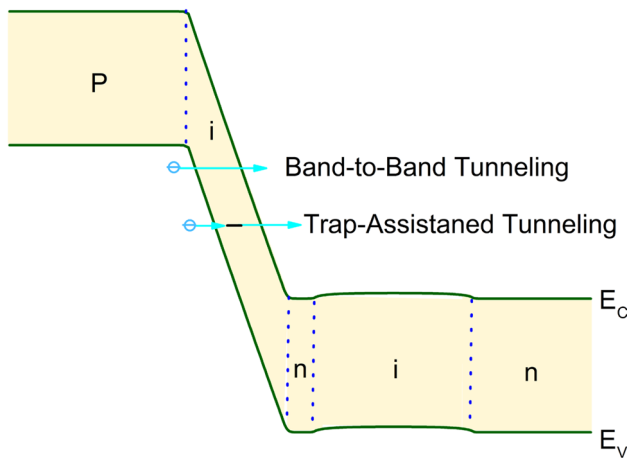


Fig. 4 Schematic illustration of the direct band-to-band tunneling and tunneling through a defect

electron hops from two centers, i and j ; $N_i(E)$ is the total number of localized states; ν_{hop} is the frequency of tunneling hops of electrons at the transport level; E is the electric field; and E_t is the localized energy.

Carriers hop through localized states in the depletion region and are believed to be associated with impurities and defects, which is identified as the main mechanism responsible for the dark conductivity of the APD [26]. At low voltage, the dark current of the APD mainly comes from carriers hopping from occupied to unoccupied sites. Therefore, the dark current of the APD is closely related to the number of localized states in the depletion region. After the GaN APD is irradiated by energetic protons, the number of localized states in the depletion region increases, so the dark current increases, and the size of dark current is related to the energies and fluences of the protons.

The band-to-band tunneling current and trap-assisted tunneling become the dominant mechanisms at the higher voltage. Both direct band-to-band tunneling and tunneling through traps in the band-gap are illustrated in Fig. 4 [27]. The current density for direct-gap semiconductors can be given by the expression [21]

$$J_{\text{bbt}} = \frac{\sqrt{2m^*} q^3 E_m V}{4\pi^2 \hbar^2 E_g^{1/2}} \exp\left(-\frac{\theta \sqrt{m^*} E_g^{3/2}}{q E_m \hbar}\right), \tag{5}$$

where E_m is the maximum junction electrical field, m^* is the electron effective mass, and θ is a parameter that depends on the detailed shape of the tunneling barrier.

When the device is under the presence of deep trap levels, the tunneling of electrons from the valence to the conduction bands is through traps, producing a trap-assisted tunneling current given by [27]

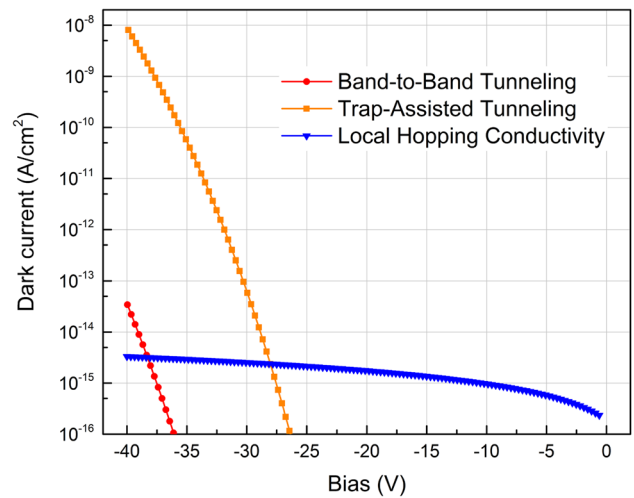


Fig. 5 Calculated dominant contributions of the different current generation mechanisms to the dark current

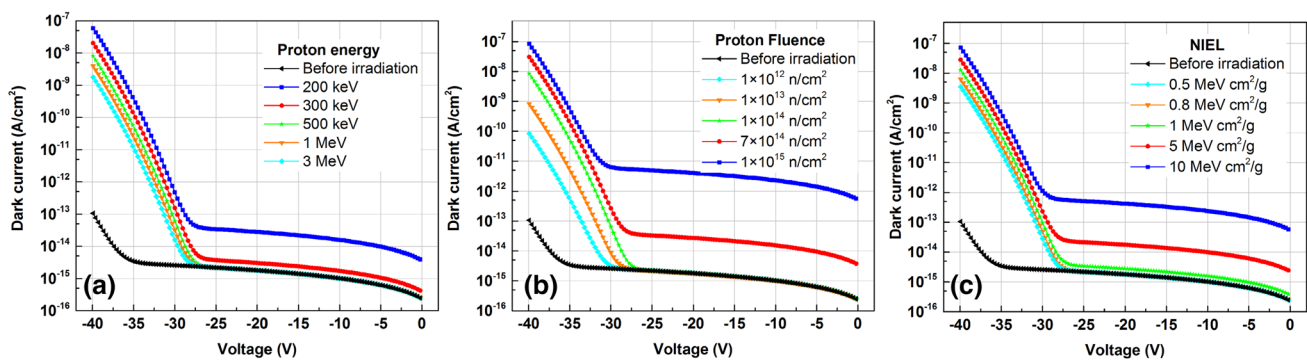
$$J_{\text{tat}} = \frac{A_d E_m V N_T \exp\left(\frac{-(B_1 E_{B1}^{3/2} + B_2 E_{B2}^{3/2})}{E_m}\right)}{N_v \exp\left(\frac{-B_1 E_{B1}^{3/2}}{E_m}\right) + N_c \exp\left(\frac{-B_2 E_{B2}^{3/2}}{E_m}\right)}, \tag{6}$$

where $A_d = q^3 \sqrt{(2m_r)/E_g} / (4\pi^3 \hbar^2)$; m_r is the reduced effective mass; $m_r = (2(m_c m_{lh})) / (m_c + m_{lh})$; m_c and m_{lh} are the conduction band effective and light-hole effective masses, respectively; $B_1 = \pi(m_{lh}/2)^{1/2} / (2q\hbar)$; $B_2 = \pi(m_c/2)^{1/2} / (2q\hbar)$; $E_{B1} = aE_g$ is the tunneling barrier height between the valence band and trap level; E_{B2} is the tunneling barrier height from the trap level to the conduction band; $E_{B2} = (1 - a)E_g$; N_v and N_c are the light-hole valence and conduction band density of states, respectively [27]; and N_T is the concentration of the traps introduced by irradiation. The value of the parameter a was assumed to be 0.25, which is the barrier height from the Ga vacancy energy level to the valence band [28–30].

Figure 5 illustrates the different contributions of the above-mentioned current generation mechanisms to the dark current when the incident proton fluence is 10^{14} n/cm² and incident energy is 300 keV. The parameters used in Fig. 5 are listed in Table 3. Since GaN is a wide band-gap material, the value of the intrinsic carrier concentration, n_i , is extremely small at room temperature. As a result, the concentrations of minority carriers (p_n and n_p) are so small that they are negligible. Therefore, the diffusion current density and generation–recombination current are insignificant in comparison with the local hopping conductivity current. As shown in Fig. 5, the local hopping conductivity current is the main part of the dark current at low voltages while the trap-assisted tunneling (TAT) current is dominant at higher voltages.

Table 3 Key parameters used in the simulation

Parameters	Electron	Hole
Mobility μ ($\text{cm}^2 \text{V}^{-1} \text{s}^{-1}$)	480	20
Diffusion coefficient D (cm^2/s)	12.48	0.52
Diffusion length L (μm)	0.35	0.07
Intrinsic carrier concentration n_i (cm^{-3})	3.26×10^{-10}	3.26×10^{-10}
depletion region width W (nm)	400	400
Lifetime τ (s)	1.0×10^{-10}	1.0×10^{-10}
Built-in potential V (V)	0.85	0.85
Junction electric field (V/cm)	2.1×10^4	2.1×10^4
Density of states N (cm^{-3})	2.65×10^{18}	3.26×10^{19}
Effective mass (relative) m	0.22	1.00

**Fig. 6** Calculated I - V characteristics with various **a** proton energies, **b** proton fluences, and **c** the NIEL

Based on the dark current generation mechanisms, the total dark current density is calculated. Figure 6 shows the dark current density before and after irradiation with (a) different incident energies at the same fluence of $5 \times 10^{14} \text{ n/cm}^2$, (b) different proton fluences at a 300 keV incident energy, and (c) different values of NIEL. In order to clearly show the relationship between the dark current density and the irradiation parameters, the dependences of the dark current density on the change of proton energy, proton fluence, and the NIEL at different voltages are plotted in Fig. 7. The values of the dark current before irradiation are plotted at an x -coordinate of zero. Clearly, the dark current density at -40 V has a larger increase than the other voltages. The fundamental reason is that different dark current generation mechanisms are dominant at different bias voltages.

At a voltage of -40 V , the main dark current generation mechanism is trap-assisted tunneling. Here, we assume the inherent vacancy density of the APD is 10^{12} cm^{-3} , and the dark current density before irradiation is 10^{-13} A/cm^2 at a -40 V reverse bias. Considering Fig. 7a as an example and combining with the results of Fig. 3a, as the protons energies increase, the average vacancy density in the multiplication region increases to $1 \times 10^{18} \text{ n/}$

cm^{-3} (200 keV) before decreasing to $5 \times 10^{17} \text{ n/cm}^{-3}$ (300 keV). As the proton energy continues to increase, the average vacancy density in the multiplication region gradually reduces to $2 \times 10^{16} \text{ n/cm}^{-3}$ (3000 keV). Correspondingly, the dark current density increases to $6 \times 10^{-7} \text{ A/cm}^2$ irradiated by 200 keV protons. With the increase in incident proton energy, the dark current reduces to $2 \times 10^{-8} \text{ A/cm}^2$ (300 keV) and continues decreasing to $2 \times 10^{-9} \text{ A/cm}^2$ (3000 keV).

At lower voltages, the dominant dark current generation mechanism is the hopping conductivity current. The key parameter affecting the hopping conductivity current is the localized states density $N_i(E)$, which includes the density-of-states tail ($2.3 \times 10^{18} \text{ cm}^{-3}$) [24] and defect states density induced by irradiation. Therefore, when the defect states density is small, there is little change in the hopping conductivity current. Only when the defect states density induced by irradiation is larger (up to $\sim 10^{18} \text{ cm}^{-3}$), will the dark current increase greatly. As shown in Fig. 7a, the dark current only increases significantly when the proton energy is small, but when the irradiation energy is large, the dark current does not change significantly. As seen in Fig. 7b, when the device is irradiated by protons at small fluences, there are no obvious changes in the dark current

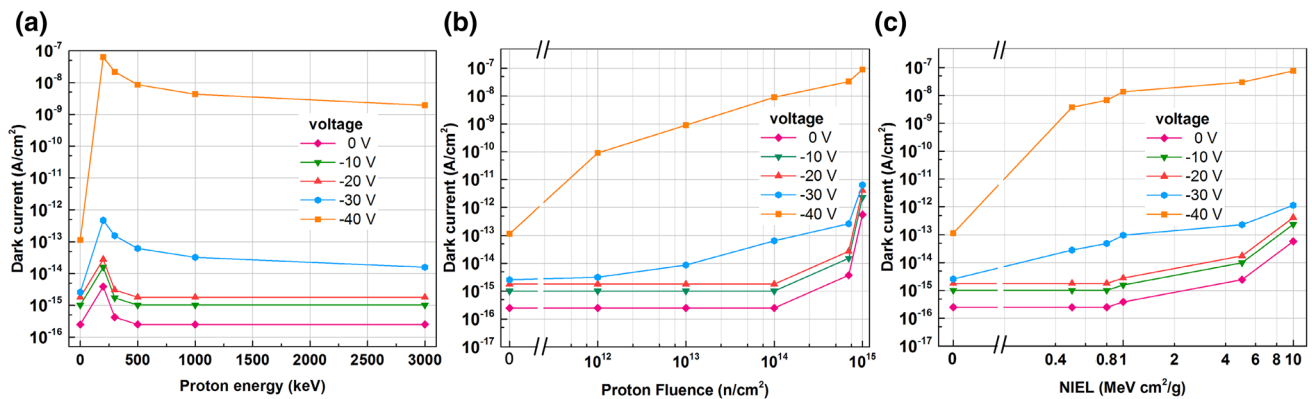


Fig. 7 Dark current density versus **a** proton energy, **b** proton fluence, and **c** the NIEL at different voltages

at low voltages. However, when the proton fluence is up to 7×10^{14} n/cm², the dark current increases quickly. In Fig. 7c, the dark current density increases with the increasing NIEL. When the NIEL is less than 1 MeV cm²/g, the dark current changes slightly. As the NIEL continues to increase, the dark current rapidly increases.

This result shows that lower proton energies, and higher fluences and NIEL induce more damage to the electrical properties of the device [31]. As reported by Kim et al. [15], protons at an energy of 15 MeV can penetrate deeper into the device, but 5 MeV protons degrade the device more severely. Therefore, we can conclude that for a proton irradiation environment with a relatively large energy, on the basis of ensuring good device performance, the thinner the device, the smaller the radiation damage.

5 Conclusion

In summary, we have studied the effects of high-energy proton irradiation on a GaN SAM APD. The vacancy density of the Ga atoms is greater than that of the N atoms induced by the radiation of proton with different energies, because of the smaller displacement energy of the Ga atoms. We found that a higher proton energy leads to a larger radiation damage area. The higher proton energy corresponds to a smaller vacancy density and NIEL at the same depth of the device. Due to the small size of the detector, the NIEL is essentially unchanged when the proton energy is greater than 500 keV and reduced at the interface of each layer in the device. We calculated the changes in dark currents of the device irradiated by different energies and fluences of protons and found that the dark current density increases with increasing proton fluences and decreasing proton energies.

References

1. J. Duboz, E. Frayssinet, S. Chenot et al., X-ray detector based on GaN. Proc. SPIE. (2013). <https://doi.org/10.1117/12.2007827>
2. H.C. Chiamori, R. Miller, A. Suria et al., Irradiation effects of graphene-enhanced gallium nitride (GaN) metal–semiconductor–metal (MSM) ultraviolet photodetectors. SPIE Sens. Technol. Appl. (2015). <https://doi.org/10.1117/12.2178091>
3. M. Chen, J.-K. Sheu, M.-L. Lee et al., Improved performance of planar GaN-based p–i–n photodetectors with Mg-implanted isolation ring. Appl. Phys. Lett. **89**, 183509 (2006). <https://doi.org/10.1063/1.2372767>
4. R.D. Dupuis, J.-H. Ryou, S.-C. Shen et al., Growth and fabrication of high-performance GaN-based ultraviolet avalanche photodiodes. J. Cryst. Growth **310**, 5217–5222 (2008). <https://doi.org/10.1016/j.jcrysgro.2008.07.107>
5. A. Ionascut-Nedelcescu, C. Carlone, A. Houdayer et al., Radiation hardness of gallium nitride. IEEE Trans. Nucl. Sci. **49**, 2733–2738 (2002). <https://doi.org/10.1109/TNS.2002.805363>
6. M. Gussenhoven, E. Mullen, D. Brautigam, Improved understanding of the Earth’s radiation belts from the CRRES satellite. IEEE Trans. Nucl. Sci. **43**, 353–368 (1996). <https://doi.org/10.1109/23.490755>
7. S. Verghese, K. McIntosh, R.J. Molnar et al., GaN avalanche photodiodes operating in linear-gain mode and Geiger mode. IEEE Trans. Electron Devices **48**, 502–511 (2001). <https://doi.org/10.1109/16.906443>
8. Y. Zhou, C. Ahyi, C.-C. Tin et al., Fabrication and device characteristics of Schottky-type bulk GaN-based “visible-blind” ultraviolet photodetectors. Appl. Phys. Lett. **90**, 121118 (2007). <https://doi.org/10.1063/1.2715114>
9. J.L. Pau, C. Bayram, R. McClintock et al., Back-illuminated separate absorption and multiplication GaN avalanche photodiodes. Appl. Phys. Lett. **92**, 101120-1–101120-3 (2008). <https://doi.org/10.1063/1.2897039>
10. M.-H. Ji, J. Kim, T. Detchprohm et al., p–i–p–i–n separate absorption and multiplication ultraviolet avalanche photodiodes. IEEE Photonics Technol. Lett. **30**, 181–184 (2018). <https://doi.org/10.1109/LPT.2017.2779798>
11. Z. Shao, D. Chen, Y. Liu et al., Significant performance improvement in AlGaIn solar-blind avalanche photodiodes by exploiting the built-in polarization electric field. IEEE J. Sel. Top. Quantum Electron. **20**, 187–192 (2014). <https://doi.org/10.1109/JSTQE.2014.2328437>
12. X. Wang, W. Hu, M. Pan et al., Study of gain and photoresponse characteristics for back-illuminated separate absorption and

- multiplication GaN avalanche photodiodes. *J. Appl. Phys.* **115**, 013103 (2014). <https://doi.org/10.1063/1.4861148>
13. J.F. Ziegler, M.D. Ziegler, J.P. Biersack, SRIM—the stopping and range of ions in matter. *Nucl. Instrum. Methods Phys Res. B Beam Interact. Mater. At.* **268**, 1818–1823 (2010). <https://doi.org/10.1016/j.nimb.2010.02.091>
 14. U. Saha, K. Devan, S. Ganesan, A study to compute integrated dpa for neutron and ion irradiation environments using SRIM-2013. *J. Nucl. Mater.* **503**, 30–41 (2018). <https://doi.org/10.1016/j.jnucmat.2018.02.039>
 15. H.-Y. Kim, J. Kim, L. Liu et al., Effects of proton irradiation energies on degradation of AlGaIn/GaN high electron mobility transistors. *J. Vac. Sci. Technol. B* **30**, 012202 (2012). <https://doi.org/10.1116/1.3676034>
 16. S.J. Pearton, R. Deist, F. Ren et al., Review of radiation damage in GaN-based materials and devices. *J. Vac. Sci. Technol. A Vac. Surf. Films* **31**, 050801 (2013). <https://doi.org/10.1116/1.4799504>
 17. S. Messenger, E. Burke, G. Summers et al., Nonionizing energy loss (NIEL) for heavy ions. *IEEE Trans. Nucl. Sci.* **46**, 1595–1602 (1999). <https://doi.org/10.1109/23.819126>
 18. I. Jun, M.A. Xapsos, S.R. Messenger et al., Proton nonionizing energy loss (NIEL) for device applications. *IEEE Trans. Nucl. Sci.* **50**, 1924–1928 (2003). <https://doi.org/10.1109/TNS.2003.820760>
 19. F. Gao, N. Chen, E. Hernandez-Rivera et al., Displacement damage and predicted non-ionizing energy loss in GaAs. *J. Appl. Phys.* **121**, 095104 (2017). <https://doi.org/10.1063/1.4977861>
 20. S.M. Sze, K.K. Ng, *Metal–semiconductor contacts. Physics of semiconductor devices* (Wiley, New York, 2006), pp. 134–196
 21. S. Forrest, R. Leheny, R. Nahory et al., In_{0.53}Ga_{0.47}As photodiodes with dark current limited by generation–recombination and tunneling. *Appl. Phys. Lett.* **37**, 322–325 (1980). <https://doi.org/10.1063/1.91922>
 22. D. Monroe, Hopping in exponential band tails. *Phys. Rev. Lett.* **54**, 146 (1985). <https://doi.org/10.1103/PhysRevLett.54.146>
 23. T. Tiedje, A. Rose, A physical interpretation of dispersive transport in disordered semiconductors. *Solid State Commun.* **37**, 49–52 (1981). [https://doi.org/10.1016/0038-1098\(81\)90886-3](https://doi.org/10.1016/0038-1098(81)90886-3)
 24. N. Bochkareva, V. Voronenkov, R. Gorbunov et al., Hopping conductivity and dielectric relaxation in Schottky barriers on GaN. *Semiconductors* **51**, 1186–1193 (2017). <https://doi.org/10.1134/S1063782617090068>
 25. C. Qiu, C. Hoggatt, W. Melton et al., Study of defect states in GaN films by photoconductivity measurement. *Appl. Phys. Lett.* **66**, 2712–2714 (1995). <https://doi.org/10.1063/1.113497>
 26. D.V. Kuksenkov, H. Temkin, Low-frequency noise and performance of GaN p–n junction photodetectors. *J. Appl. Phys.* **83**, 2142–2146 (1998). <https://doi.org/10.1063/1.366950>
 27. J.P. Donnelly, E.K. Duerr, K.A. McIntosh et al., Design considerations for 1.06- μm InGaAsP–InP Geiger-mode avalanche photodiodes. *IEEE J. Quantum Electron.* **42**, 797–809 (2006). <https://doi.org/10.1109/JQE.2006.877300>
 28. P. Muret, A. Philippe, E. Monroy et al., Properties of a hole trap in n-type hexagonal GaN. *J. Appl. Phys.* **91**, 2998–3001 (2002). <https://doi.org/10.1063/1.1433935>
 29. D.C. Look, Defect-related donors, acceptors, and traps in GaN. *Phys. Status Solidi B* **228**, 293–302 (2001). [https://doi.org/10.1002/1521-3951\(200111\)228:1%3c293:aid-pssb293%3e3.0.co;2-f](https://doi.org/10.1002/1521-3951(200111)228:1%3c293:aid-pssb293%3e3.0.co;2-f)
 30. M.A. Reshchikov, H. Morkoç, Luminescence properties of defects in GaN. *J. Appl. Phys.* **97**, 5–19 (2005). <https://doi.org/10.1063/1.1868059>
 31. S.-F. Tang, H.-H. Hsieh, H.-Y. Tu et al., Investigations for InAs/GaAs multilayered quantum-dot structure treated by high energy proton irradiation. *Thin Solid Films* **518**, 7425–7428 (2010). <https://doi.org/10.1016/j.tsf.2010.05.009>